ARTICLE

Reversible Attachment of Platinum Alloy Nanoparticles to Nonfunctionalized Carbon Nanotubes

Beate Ritz,[†] Hauke Heller,[†] Anton Myalitsin,[†] Andreas Kornowski,[†] Francisco J. Martin-Martinez,[‡] Santiago Melchor,[‡] Jose A. Dobado,[‡,*] Beatriz H. Juárez,[§] Horst Weller,[†,*] and Christian Klinke[†,*]

[†]Institute of Physical Chemistry, University of Hamburg, 20146 Hamburg, Germany, [‡]Department of Organic Chemistry, University of Granada, 18071 Granada, Spain, and [§]IMDEA Nanoscience, 28049 Madrid, Spain

ABSTRACT The formation of monodisperse, tunable sized, alloyed nanoparticles of Ni, Co, or Fe with Pt and pure Pt nanoparticles attached to carbon nanotubes has been investigated. Following homogeneous nucleation, nanoparticles attach directly to nonfunctionalized single-walled and multi-walled carbon nanotubes during nanoparticle synthesis as a function of ligand nature and the nanoparticle work function. These ligands not only provide a way to tune the chemical composition, size, and shape of the nanoparticles but also control a strong reversible interaction with carbon nanotubes and permit controlling the nanoparticle coverage. Raman spectroscopy reveals that the sp^2 hybridization of the carbon lattice is not modified by the attachment. In order to better understand the interaction between the directly attached nanoparticles and the nonfunctionalized carbon nanotubes, we employed first-principles calculations on model systems of small Pt clusters and both zigzag and armchair single-walled carbon nanotubes. The detailed comprehension of such systems is of major importance since they find applications in catalysis and energy storage.

KEYWORDS: nanoparticles · nanocrystals · nanotubes · composites · platinum · alloys · DFT · colloidal chemistry

Composites of metallic nanoparticles (NPs) and carbon nanotubes (CNTs) exhibit high catalytic activity for various chemical reactions[1−6] and have also been explored for hydrogen storage applications.[7] Recent reports include platinum,[6,8,9] cobalt,[10,11] nickel,[7,12] gold,[13] rhodium,[14] as well as platinum nickel,[15] platinum tin,[16] and platinum ruthenium[17] NPs immobilized on CNTs.[18] Alloying NPs of platinum with nickel, cobalt, or iron allows tunable magnetic response[19,20] and catalytic properties.[21−23] Beyond that, 1D alignment of NPs enables one to modify the saturation magnetization and coercitivity through magnetostatic coupling.[24−26] A convenient method for 1D alignment is the attachment of NPs to CNTs, which is usually achieved by electrochemical deposition,[27,28] the reduction of metallic salts in the presence of functionalized CNTs,[15,29] or chemical vapor deposition,[10] among others.[30] On the other hand, concerning the NP synthesis, the organometallic synthesis route provides nanocrystalline alloyed materials with precise size control and tunable composition in several systems.[20,31,32] Here, we report the synthesis of alloyed Ni_xPt_{1-x},[20] Co_xPt_{1-x}, and Fe_xPt_{1-x}[32] NPs as well as pure Pt[33] NPs and their attachment to nonfunctionalized single-walled carbon nanotubes (SWCNTs), multi-walled carbon nanotubes (MWCNTs), and glassy carbon by their simple integration in the organometallic synthesis. The experimental procedure involves only a single synthetic step, whereby the crucial parameter for attachment was found in the correct balance of the ligands oleylamine (OA) and oleic acid (Oac). Under the appropriate conditions, only poorly stabilized NPs are formed, which enables the CNTs to act as additional ligands as it was previously observed for the CdSe−CNT system.[34−36] Additionally, we present first-principles calculations, indicating a charge transfer from the CNTs to the NPs upon attachment, resulting in positive charging of the CNTs. These findings are understood in terms of Fermi level equilibration leading to an electrostatic stabilization of the composite material.

The composites were synthesized by the reduction or thermal decomposition of the metal precursors in the presence of CNTs or glassy carbon, OA or a mixture of OA and Oac, and 1,2-hexadecanediol in diphenyl ether at 200 °C (see Experimental Details). We have synthesized a large variety of NPs attached to CNTs with different sizes and compositions. Some examples are listed in Table 1 (further ones can be found in the Supporting Information).

All alloy samples consist of monodisperse NPs densely covering the surface of the CNTs. Such high coverage was also ob-

*Address correspondence to dobado@ugr.es, weller@chemie.uni-hamburg.de, klinke@chemie.uni-hamburg.de.

Received for review February 5, 2010 and accepted February 28, 2010.

Published online March 5, 2010. 10.1021/nn100240c

served for pure Pt NPs, which are, however, rather polydisperse (TEM images and XRD shown in the Supporting Information S1−S3). To follow the process in more detail, we took aliquots from the reaction mixture after different times. Representative TEM images are shown in Figure 1 for the NiPt−CNT system after 1 and 10 min of reaction. As reported for the particle synthesis in homogeneous solution, the particle formation is fast and the reaction is usually finished within a few minutes after the injection of the platinum precursor.[20,32,37−39] Accordingly, we find a large amount of small particles either freely in solution or covering the CNTs already after 1 min of synthesis. In the next minutes, the particles grow both in solution and on the CNTs, which are homogeneously and densely covered with NPs after 10 min (Figure 1b). It is, therefore, most likely that homogeneous nucleation occurs in solution followed by an attachment to the CNTs, although partial nucleation on the CNTs cannot be excluded. Such composites are stable at least over months and endure ultrasound treatment for at least 24 h.

HRTEM images of CoPt NPs attached to SWCNTs (Figure 2) show an atomically close proximity of the NP and the CNT surface, while there is a visible distance of about 0.8 nm between two adjacent NPs due to the ligands on the NP surfaces. The NPs are closely connected to the CNTs' surface with no apparent ligands between. Thus, the facet connected to the CNTs may lack ligands, allowing direct connection between the NP surface and the CNT. Analysis of the crystal orientation reveals that the particles attach *via* the {100} facets. This seems plausible when one keeps in mind the nearly cubic shape of the particles. Detailed investigations on small, almost spherical particles show, however, that the attachment also occurs selectively *via* the {100} facet. HRTEM images with the corresponding FFTs and electron diffraction are shown in the Supporting Information S4 and S5.

The role of Oac and OA on the nucleation and growth of platinum alloy particles has been investigated by several authors.[20,37−42] Consistently, it was found that OA is essential to obtain stable colloidal solutions of nanoparticles showing defined size, shape, and composition, whereas Oac influences their composition and size. The nonexisting contribution of Oac on the attachment that we found in our experiments produces highly covered NP−CNT composites with tunable size and composition of the NPs (exemplary for NiPt−MWCNT composites shown in the Supporting Information S6−S8). Further, we found that OA additionally controls the immobilization of the NPs on the CNTs. This can be clearly seen in the TEM images in Figure 3. While comparably low OA concentrations (see Experimental Details) yield highly covered CNTs even if a high Oac concentration is used (Figure 3a), higher concentrations of OA produce aggregated or separated NPs in solution (Figure 3b), preventing further attachment.

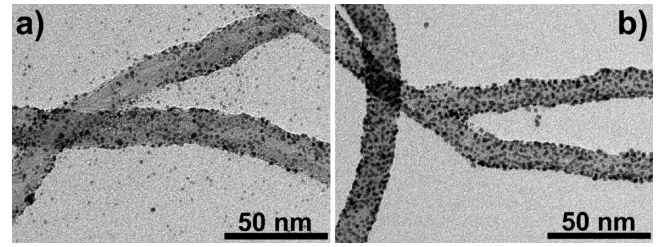

Figure 1. TEM images of NiPt−CNT composites 1 min (a) and 10 min (b) after the injection of the platinum precursor.

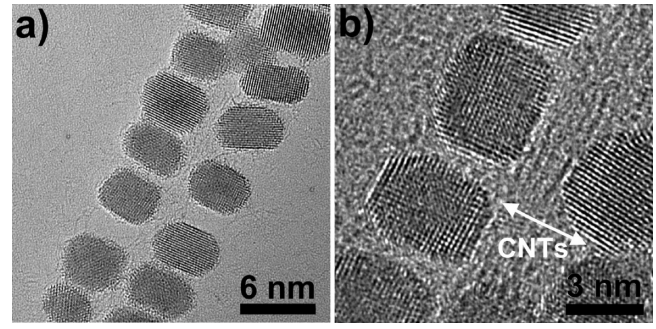

Figure 2. HRTEM images of CoPt NPs attached to SWCNTs.

It is worth mentioning that the addition of excess OA to a sample with a high coverage of NPs (prepared with 0.15 mmol OA) results in spontaneous detachment of the particles from the CNTs (Figure 4b). In contrast, the addition of the same amount of Oac does not influence the attachment significantly (Figure 4a). Accordingly, it is possible not only to remove the NPs from the surface of CNTs but also to attach them in a postsynthesis procedure. NPs insufficiently stabilized by OA mixed with CNTs yield similar composites due to the stabilization of the NPs by the CNTs (see Experimental Details and Supporting Information S9).

We therefore conclude that the strong binding of OA to Pt competes with the NPs anchoring to CNTs. In this sense, NP attachment to the graphene-like system CNTs can be understood as a ligand exchange process as already described for a CdSe−CNT system.[35] In the Supporting Information, we show that the attachment also applies to other sp^2-hybridized carbon systems such as glassy carbon (Supporting Information S11).

In order to learn more about the type of interaction between NPs and CNTs, Raman spectroscopy was performed. The features analyzed here are the disorder-induced mode (D-band) and the graphene-like tangential displacement mode (G-band), as shown in Figure 5 for the Nanocyl SWCNTs used in this study. SWCNTs were probed using an Ar−Kr laser at two different wavelengths of 514.5 nm (2.41 eV) and 647.1 nm (1.92 eV). The lower wavelength was primarily resonant with the semiconducting fraction of the Nanocyl SWCNTs employed in this study, while the higher wavelength was mainly resonant with the metallic fraction. The D mode corresponds to the sp^3 hybridization of the CNTs and is sensitive to covalent functionalization.[43] The ob-

TABLE 1. Optimized Ligand-to-Metal Ratios (in 10 mL of Diphenyl Ether in the Presence of 2 mg of CNTs) for Different Metal Precursors and NP Composition

#	metal precursor	Oac [mmol]	Oac/Me	OA [mmol]	OA/Me	OA/total Me (including Pt)	diameter [nm]	composition
1	$Ni(ac)_2$			0.15	1	0.5	5.5 ± 0.7	$Ni_{46}Pt_{54}$
2	$Co_2(CO)_8$	6.3	38	0.15	1	0.5	4.9 ± 0.9	Co_9Pt_{91}
3	$CoCl_2 \cdot 6H_2O$			0.15	1	0.5	6.9 ± 1.2	$Co_{19}Pt_{81}$
4	$CoCl_2 \cdot 6H_2O$			0.30	2	1	9.3 ± 1.7	$Co_{31}Pt_{69}$
5	$Fe(CO)_5$			0.15	1	0.5	3.4 ± 0.4	$Fe_{40}Pt_{60}$
6	$Pt(acac)_2$	0.15	1	0.15	1	1	2−10	Pt

served intensity changes of the D-band relative to the sum of the D- and G-band upon immobilization of NPs (see Supporting Information S10) were within the error bars of the respective experiments, in the cases of primarily probing semiconducting and metallic SWCNTs. If covalent functionalization of the CNT structure occurred, the intensity of the D-band would increase significantly. We therefore consider these changes negligible and conclude that mainly noncovalent bonding took place. Thus, the sp^2 structure of the CNTs is preserved during the formation of NP−CNT composites.

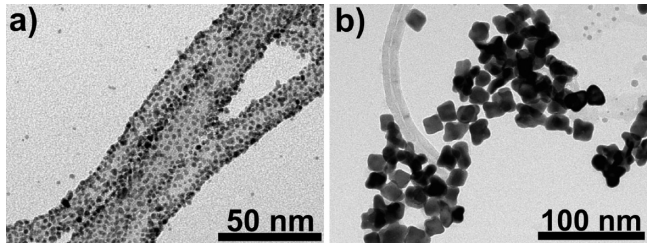

Figure 3. NiPt-based NP−CNT composites synthesized with (a) 6.3 mmol Oac and 0.15 mmol OA and (b) 6.1 mmol OA.

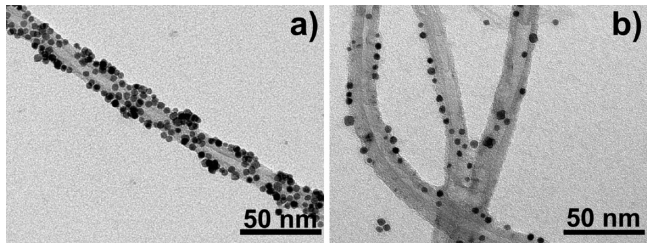

Figure 4. NiPt−MWCNT composites (Figure 1b) sonicated with Oac (a) and same amount of OA (b). Untreated composites are shown in the Supporting Information S6a.

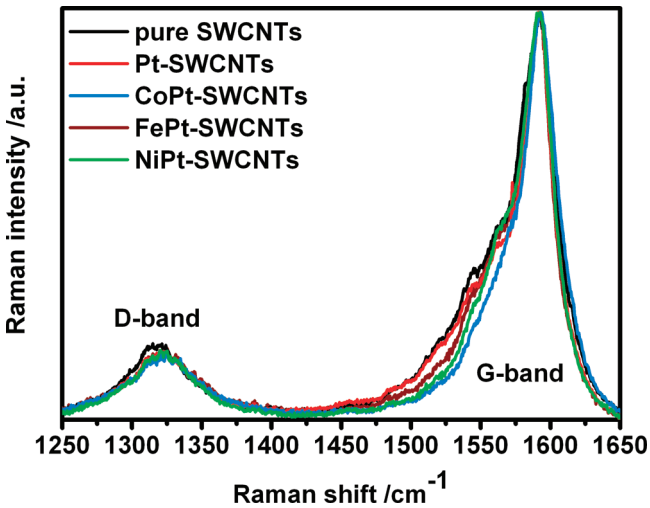

Figure 5. D- and G-bands of pristine SWCNTs and NP−SWCNT composites with high loads of FePt, CoPt, NiPt, and Pt NPs using a laser energy of 2.41 eV.

Further information about the nature of the interaction between NPs and CNTs can be gained by first-principles theoretical calculations. We modeled systems of small Pt clusters on both zigzag and armchair CNTs. The interaction between Pt and CNTs has been previously analyzed in the literature employing tight-binding[44,45] and plane-wave calculations.[46] However, for a detailed analysis, advanced tools for bond nature characterization such as quantum theory of atoms in molecules (QTAIM)[47] or electron localization function (ELF)[48] are necessary. Thus, we calculated optimized geometries and total energies by density functional theory (DFT) methods, employing the hybrid B3LYP functional,[49,50] together with the LanL2DZ ECP basis set with effective core potentials for Pt atoms[51−55] and the STO-3G one for C and H atoms.[56,57] In order to analyze the charge transfer and the bonding nature of the interaction, molecular electrostatic potential (MEP), QTAIM, and ELF[48] have been employed. Due to a more accurate description of the electron density of localized electrons in bonds, we chose a finite molecular model rather than a periodic system. As a matter of fact, finite and periodic models differ sometimes in the resulting geometry of isolated CNTs.[58] Thus, we checked the current geometric results with the reported periodic ones.[46] The final model system consists of a pyramidal cluster composed by 14 Pt atoms over the surface of a (10,0) CNT (see Figure 6).[59] We have also explored other CNTs such as (12,0), (5,5), and (6,6) for comparison, but the results are similar in all cases. Therefore, we focus the discussion on (10,0) CNTs.

First, we fully optimized all of the different configurations between one Pt atom and the (10,0) CNT to obtain the preferred absorption spots and the Pt−C equilibrium distance, which has been compared with the results using periodic boundary conditions. One Pt atom can be placed over a C atom of the CNT, above a bond, or above a center of a carbon ring. However, due to the CNT topology, two different bonds have to be considered, those in the axis direction and those in a certain angle with the axis direction, resulting in four different configurations. Optimization showed that the Pt atoms above C−C bonds are the preferred position

with a Pt−C distance of 2.0 Å in accordance with ref 46. Subsequently, we constructed a 3 × 3 atom sheet in {100} and {111} fcc facet configuration over a CNT with an angle of 0, 30, and 45° relative to each other. We explored the potential energy surface with a single-point energy calculations scan for 24 different combinations[60] using the Pt−C distance obtained in the previous step. Using this nine Pt atom cluster (one shell) in {100} and {111} fcc arrangement, the calculations showed that the interactions with the {100} facets are the preferred ones, supporting the experimental results. The lowest energy situation is the one in which the central atom in the nine atom {100} facets is placed on top of the bond in axis direction and the angle between the cluster and the CNT is 45°. This situation allows a high number of Pt atoms to match on top of bonds and C atoms (preferred positions) rather than on rings. The minimum energy configuration was further optimized with a fixed 14 Pt atom cluster pyramid (using 2.7 Å for the Pt−Pt distance). With this model system, it is observed that the CNT is slightly deformed toward the Pt cluster. This provides evidence for the attraction between Pt and CNTs. Moreover, this deformation is highlighted not only from a geometrical point of view but also from an electronic one. In Figure 6a, the MEP plot shows clearly more negative values around the platinum cluster in interaction with the CNT (red isosurface), which is even more noteworthy if we look at the MEP distribution of the isolated cluster (inset of Figure 6a), in which a nonhomogeneous distribution is presented. This fact, together with the emptied MEP isosurface in the region of the CNT opposite to the cluster (in yellow), suggests a charge transfer from the CNT to the cluster, as we expected since the value of the Pt work function is higher than the one of C.

The work functions of semiconducting and metallic SWCNTs are 4.8−5.4 and 4.5−5.0 eV, respectively.[61] While Pt features a work function of 5.65 eV (averaged values from Landolt−Börnstein), those of Ni and Co are considerably lower with 5.15 and 5.0 eV. Finally, the value of Fe is even lower with 4.5 eV. The resulting work functions for the alloys should be between the value of platinum and the respective metal, depending on the composition and crystal structure of the alloys. The computational results together with the values for the work functions show that charge transfer from the SWCNTs to the platinum alloys is plausible unless the iron content is too high. Calculated binding energies for single atoms to CNTs further support our results. Spin-polarized binding energies of 2.4 eV for a single platinum atom, 1.7 eV for a single cobalt or nickel atom, and finally 0.8 eV in the case of a single iron atom are reported.[62] On the other hand, ELF calculations show weak electron localization in the path from C to Pt (Figure 6b), which implies a small covalent contribution to the bond, although too small and sparse to be seen in Raman spectroscopy. Thus, according to theoretical calculations, the {100} fcc facet is the most stable one for the interaction, arising from a charge transfer from the CNT to the metal that rules the attachment with a small covalent contribution, causing a geometrical deformation of the CNT structure.

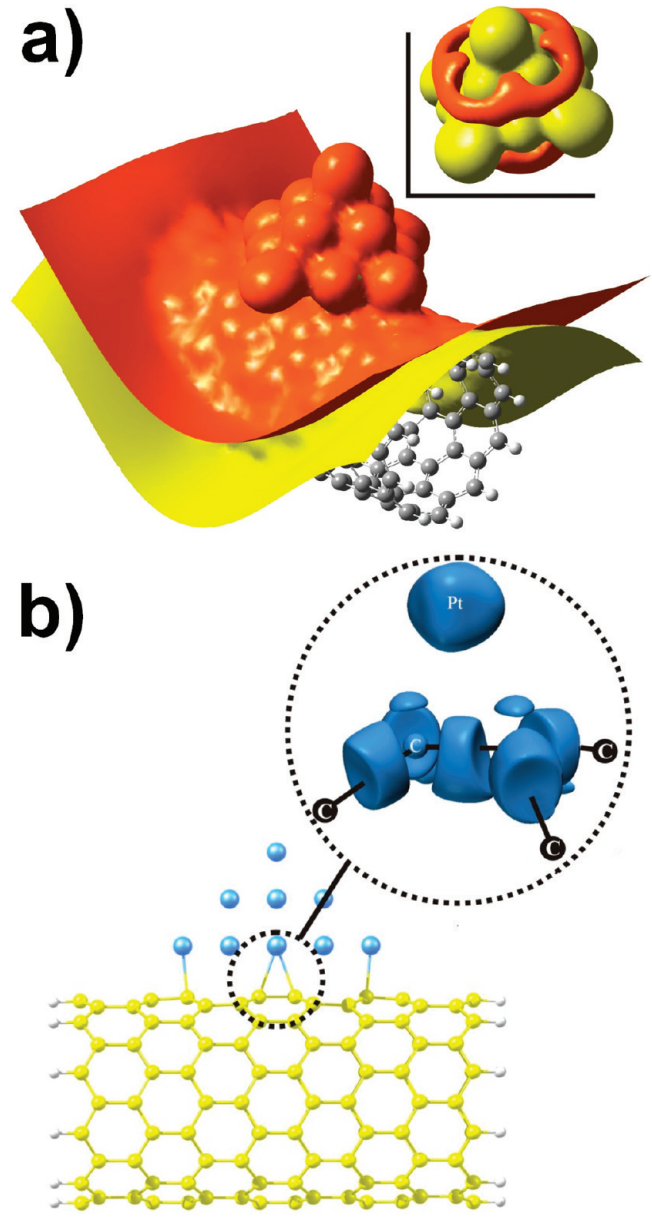

Figure 6. Models of 14 Pt atoms on a (10,0) SWCNT. (a) MEP plot of the composite and an isolated Pt cluster in the inset. Red indicates a surface of constant negative potential and yellow a positive one. (b) With an ELF analysis showing the paired electron density in blue. Small kidney-shaped islands can be found between the carbon lattice and the Pt cluster, indicating a minor covalent contribution. In contrast, strong covalent bonds are localized between the carbon atoms.

Summarizing, we have shown that fine-tuning of the concentration of oleic acid and oleylamine allows control over not only the size, shape, and composition of Pt-based nanoparticles but also their re-

versible attachment to CNTs. Computational investigations provided evidence for a charge stabilization of the composites. The work functions of platinum-based NPs are lower than those of the CNTs leading to a charge transfer from the CNTs to the NPs until the Fermi levels are equilibrated. The different polarization of the materials provides the attractive forces responsible for the charge stabilization, while the electronic structure of the CNTs is preserved. Such composites may find applications in fuel cells or energy storage. The knowledge about the involved mechanism of reversible attachment might help to develop composite systems with NPs of different nature.

EXPERIMENTAL DETAILS

The synthesis was carried out under a nitrogen atmosphere. In a typical synthesis of spherical $Ni_{40}Pt_{60}$ particles attached to CNTs, $Ni(ac)_2$ (41.6 mg), 1,2-hexadecanediol (43.0 mg), oleylamine (0.05 mL), and diphenyl ether (8 mL) were mixed in a three-neck flask equipped with a reflux condenser, septum, and a heat controller. The mixture was kept at 80 °C for 1 h under vacuum conditions to remove traces of water. Then the CNTs or the glassy carbon spheres (from 1 to 10 mg) suspended in diphenyl ether (1−5 mL) by sonication were added and conditioned again. The mixture was then heated to 200 °C under nitrogen atmosphere, and $Pt(acac)_2$ (65.5 mg) dissolved in 1,2-dichlorobenzene (0.6 mL) was injected amid vigorous stirring. The black dispersion was stirred for 2 h. The reaction mixture was cooled to room temperature, and chloroform (10 mL) was added under ambient conditions. The CNT composites were isolated by centrifugation. The precipitate was dispersed in chloroform and washed two times.

The synthesis of $Co_{19}Pt_{81}$ CNT composites with $CoCl_2 \cdot 6H_2O$ and $Fe_{40}Pt_{60}$ with $Fe(CO)_5$ as the source of cobalt or iron is comparable. If $Co_2(CO)_8$ is used, we need higher amounts of Oac to get CNT composites as described above, and the $Co_2(CO)_8$ has to be injected in the hot solution, as well.

Post-synthesis Procedure. For the attachment of NPs in a post-synthesis step, the NPs were washed after the synthesis six times with chloroform and methanol. Then the particles were suspended in 2 mL of diphenyl ether and injected in a solution containing 2 mg of CNTs in 8 mL of diphenyl ether and 0.05 mL of oleylamine at 200 °C. After stirring this mixture for 2 h at 200 °C, the composites were washed with chloroform. (TEM images are shown in the Supporting Information S9).

Ligand Exchange. Treatment of the NP−CNT composites by ultrasonication in the presence of OA leads to nearly complete detachment of the NPs already after a few minutes. If the NP−CNT composites are ultrasonicated with the same amount of Oac, the NPs persist on the CNTs. Although there is also some detachment visible, it is a lot less pronounced (TEM images shown in Figure 4). Without supplemental ligands, the composites are stable over more than 24 h treating by ultrasonication.

Methods. The composites were characterized by high-resolution transmission electron microscopy with a JEOL JEM 1011 at an acceleration voltage of 100 kV, Philips CM 300 UT at an acceleration voltage of 200 kV, and a JEOL JEM 2200 FS (UHR) with CESCOR and CETCOR corrector at an acceleration voltage of 200 kV. The composition of the particles was determined by energy-dispersive X-ray spectroscopy (EDX) with an EDAX detector (DX4) spectrometer connected to the Philips CM 300 UT. Samples for TEM analysis were prepared by drying a dispersion of the CNT composite in chloroform on a carbon-coated copper grid. Sample preparation for XRD measurements involved dropping the dispersion on a single-crystal Si support and evaporating the solvent. The X-ray diffractograms were recorded on a Philips X'Pert diffractometer with Bragg−Brentano geometry and Cu Kα radiation.

For the Raman spectroscopy measurements, the composites were dropped on a silicon wafer and the chloroform was evaporated. The experiments were performed using Ar−Kr laser lines of 514.5 nm (2.41 eV) or 647.1 nm (1.92 eV with a high numerical aperture Zeiss Epiplan Apochromat objective (150×, NA = 0.95). The laser power was 2.5 mW, corresponding to 2 MW/cm^2, while the grating employed had 1200 grooves/mm.

Computational Methods. The DFT calculations were carried out with Gaussian03[63] and NWChem 5.1,[64] while the construction of CNTs was performed with the CoNTub 1.0 program.[65,66]

Acknowledgment. This work was financially supported by the "Landesexzellenzinitiative Spintronics" (Hamburg), the Deutsche Forschungsgemeinschaft (GK 611), the Spanish "Ministerio de Ciencia e Innovación" (CTQ2007-65112, MAT2009-13488, S2009MAT-1726), and the "Ramón y Cajal" programme. We also thank the "Centro de Servicios de Informática y Redes de Comunicaciones" (CSIRC), University of Granada, for the use of the UGRGrid computing facilities.

Supporting Information Available: Additonal figures and experimental details. This material is available free of charge *via* the Internet at http://pubs.acs.org.

REFERENCES AND NOTES

1. Wildgoose, G. G.; Banks, C. E.; Compton, R. G. Metal Nanoparticles and Related Materials Supported on Carbon Nanotubes. Methods and Applications. *Small* **2006**, *2*, 182–193.
2. Zhao, Y.; Fan, L.; Zhong, H.; Li, Y.; Yang, S. Platinum Nanoparticle Clusters Immobilized on Multiwalled Carbon Nanotubes: Electrodeposition and Enhanced Electrocatalytic Activity for Methanol Oxidation. *Adv. Funct. Mater.* **2007**, *17*, 1537–1541.
3. Arico, A. S.; Srinivasan, S.; Antonucci, V. DMFCs: from Fundamental Aspects to Technology Development. *Fuel Cells* **2001**, *1*, 133–161.
4. Kongkanand, A.; Kuwabata, S.; Girishkumar, G.; Kamat, P. Single-Wall Carbon Nanotubes Supported Platinum Nanoparticles with Improved Electrocatalytic Activity for Oxygen Reduction Reaction. *Langmuir* **2006**, *22*, 2392–2396.
5. Wang, J. J.; Yin, G. P.; Zhang, J.; Wang, Z. B.; Gao, Y. Z. High Utilization Platinum Deposition on Single-Walled Carbon Nanotubes as Catalysts for Direct Methanol Fuel Cell. *Electrochim. Acta* **2007**, *52*, 7042–7050.
6. Liu, Z.; Lin, X.; Lee, J. Y.; Zhang, W.; Han, M.; Gan, L. M. Preparation and Characterization of Platinum-Based Electrocatalysts on Multi-Walled Carbon Nanotubes for Proton Exchange Membrane Fuel Cells. *Langmuir* **2002**, *18*, 4054–4060.
7. Kim, H.-S.; Lee, H.; Han, K.-S.; Kim, J.-H.; Song, M.-S.; Park, M.-S.; Lee, J.-Y.; Kang, J.-K. Hydrogen Storage in Ni Nanoparticle-Dispersed Multiwalled Carbon Nanotubes. *J. Phys. Chem. B* **2005**, *109*, 8983–8986.
8. Yang, D.-Q.; Sun, S.; Dodelet, J.-P.; Sacher, E. A Facile Route for the Self-Organized High-Density Decoration of Pt Nanoparticles on Carbon Nanotubes. *J. Phys. Chem. C* **2008**, *112*, 11717–11721.
9. Sanles-Sobrido, M.; Correa-Duarte, M. A.; Carregal-Romero, S.; Rodriguez-Gonzalez, B.; Alvarez-Puebla, R. A.; Herves, P.; Liz-Marzan, L. M. Highly Catalytic Single-Crystal Dendritic Pt Nanostructures Supported on Carbon Nanotubes. *Chem. Mater.* **2009**, *21*, 1531–1535.
10. Zhang, H.; Qiu, J.; Liang, C.; Li, Z.; Wang, X.; Wang, Y.; Feng, Z.; Li, C. A Novel Approach to Co/CNTs Catalyst *via* Chemical Vapor Deposition of Organometallic Compounds. *Catal. Lett.* **2005**, *101*, 211–214.

11. Dong, Z.; Ma, K.; He, J.; Wang, J.; Li, R.; Ma, J. Decorating Carbon Nanotubes with Cobalt Nanoparticles. *Mater. Lett.* **2008**, *62*, 4059–4061.
12. Ang, L.-M.; Hor, T. S. A.; Xu, G.-Q.; Tung, C.-h.; Zhao, S.; Wang, J. L. S. Electroless Plating of Metals onto Carbon Nanotubes Activated by a Single-Step Activation Method. *Chem. Mater.* **1999**, *11*, 2115–2118.
13. Raghuveer, M. S.; Agrawal, S.; Bishop, N.; Ramanath, G. Microwave-Assisted Single-Step Functionalization and in Situ Derivatization of Carbon Nanotubes with Gold Nanoparticles. *Chem. Mater.* **2006**, *18*, 1390–1393.
14. Giordano, R.; Serp, P.; Kalck, P.; Kihn, Y.; Schreiber, J.; Marhic, C.; Duvail, J.-L. Preparation of Rhodium Catalysts Supported on Carbon Nanotubes by a Surface Mediated Organometallic Reaction. *Eur. J. Inorg. Chem.* **2003**, *4*, 610–617.
15. Zhao, Y.; E, Y.; Fan, L.; Qiu, Y.; Yang, S. A New Route for the Electrodeposition of Platinum−Nickel Alloy Nanoparticles on Multi-Walled Carbon Nanotubes. *Electrochim. Acta* **2007**, *52*, 5873–5878.
16. Zhao, X.; Li, W.; Jiang, L.; Zhou, W.; Xin, Q.; Yi, B.; Sun, G. Multi-Wall Carbon Nanotube Supported Pt−Sn Nanoparticles as an Anode Catalyst for the Direct Ethanol Fuel Cell. *Carbon* **2004**, *42*, 3263–3265.
17. Li, L.; Xing, Y. Pt−Ru Nanoparticles Supported on Carbon Nanotubes as Methanol Fuel Cell Catalysts. *J. Phys. Chem. C* **2007**, *111*, 2803–2808.
18. Xue, B.; Chen, P.; Hong, Q.; Lin, J.; Tan, K. L. Growth of Pd, Pt, Ag and Au Nanoparticles on Carbon Nanotubes. *J. Mater. Chem.* **2001**, *11*, 2378–2381.
19. Chen, M.; Nikles, D. E. Synthesis of Spherical FePd and CoPt Nanoparticles. *J. Appl. Phys.* **2002**, *91*, 8477–8479.
20. Ahrenstorf, K.; Albrecht, O.; Heller, H.; Kornowski, A.; Goerlitz, D.; Weller, H. Colloidal Synthesis of Ni_xPt_{1-x} Nanoparticles with Tuneable Composition and Size. *Small* **2007**, *3*, 271–274.
21. Abdel Rahim, M. A.; Hassan, H. B.; Abdel Hameed, R. M. Graphite Electrodes Modified with Platinum−Nickel Nano-Particles for Methanol Oxidation. *Fuel Cells* **2007**, *7*, 298–305.
22. Yang, H.; Vogel, W.; Lamy, C.; Alonso-Vante, N. Structure and Electrocatalytic Activity of Carbon-Supported Pt−Ni Alloy Nanoparticles toward the Oxygen Reduction Reaction. *J. Phys. Chem. B* **2004**, *108*, 11024–11034.
23. Paulus, U. A.; Wokaun, A.; Scherer, G. G.; Schmidt, T. J.; Stamenkovic, V.; Radmilovic, V.; Markovic, N. M.; Ross, P. N. Oxygen Reduction on Carbon-Supported Pt−Ni and Pt−Co Alloy Catalysts. *J. Phys. Chem. B* **2002**, *106*, 4181–4191.
24. Xiong, Y.; Chen, Q.; Tao, N.; Ye, J.; Tang, Y.; Feng, J.; Gu, X. The Formation of Legume-like Structures of Co Nanoparticles through a Polymer-Assisted Magnetic-Field-Induced Assembly. *Nanotechnology* **2007**, *18*, 345301/1–345301/5.
25. Petit, C.; Russier, V.; Pileni, M. P. Effect of the Structure of Cobalt Nanocrystal Organization on the Collective Magnetic Properties. *J. Phys. Chem. B* **2003**, *107*, 10333–10336.
26. Dumestre, F.; Chaudret, B.; Amiens, C.; Respaud, M.; Fejes, P.; Renaud, P.; Zurcher, P. Unprecedented Crystalline Super-Lattices of Monodisperse Cobalt Nanorods. *Angew. Chem., Int. Ed.* **2003**, *42*, 5213–5216.
27. Kim, H.; Jeong, N. J.; Lee, S. J.; Song, K. S. Electrochemical Deposition of Pt Nanoparticles on CNTs for Fuel Cell Electrode. *Korean J. Chem. Eng.* **2008**, *25*, 443–445.
28. Quinn, B. M.; Dekker, C.; Lemay, S. G. Electrodeposition of Noble Metal Nanoparticles on Carbon Nanotubes. *J. Am. Chem. Soc.* **2005**, *127*, 6146–6147.
29. Lordi, V.; Yao, N.; Wei, J. Method for Supporting Platinum on Single-Walled Carbon Nanotubes for a Selective Hydrogenation Catalyst. *Chem. Mater.* **2001**, *13*, 733–737.
30. Georgakilas, V.; Gournis, D.; Tzitzios, V.; Pasquato, L.; Guldi, D. M.; Prato, M. Decorating Carbon Nanotubes with Metal or Semiconductor Nanoparticles. *J. Mater. Chem.* **2007**, *17*, 2679–2694.
31. Shevchenko, E. V.; Talapin, D. V.; Rogach, A. L.; Kornowski, A.; Haase, M.; Weller, H. Colloidal Synthesis and Self-Assembly of $CoPt_3$ Nanocrystals. *J. Am. Chem. Soc.* **2002**, *124*, 11480–11485.
32. Sun, S.; Murray, C. B.; Weller, D.; Folks, L.; Moser, A. Monodisperse FePt Nanoparticles and Ferromagnetic FePt Nanocrystal Superlattices. *Science* **2000**, *287*, 1989–1992.
33. Xu, C.; Wang, B.; Sun, S. Dumbbell-like Au-Fe_3O_4 Nanoparticles for Target-Specific Platin Delivery. *J. Am. Chem. Soc.* **2009**, *131*, 4216–4217.
34. Juarez, B. H.; Klinke, C.; Kornowski, A.; Weller, H. Quantum Dot Attachment and Morphology Control by Carbon Nanotubes. *Nano Lett.* **2007**, *7*, 3564–3568.
35. Juarez, B. H.; Meyns, M.; Chanaewa, A.; Cai, Y.; Klinke, C.; Weller, H. Carbon Supported CdSe Nanocrystals. *J. Am. Chem. Soc.* **2008**, *130*, 15282–15284.
36. Hungria, A. B.; Juarez, B. H.; Klinke, C.; Weller, H.; Midgley, A. P. 3-D Characterization of CdSe Nanoparticles Attached to Carbon Nanotubes. *Nano Res.* **2008**, *1*, 89–97.
37. Ahrenstorf, K.; Heller, H.; Kornowski, A.; Broekaert, J. A. C.; Weller, H. Nucleation and Growth Mechanism of Ni_xPt_{1-x} Nanoparticles. *Adv. Funct. Mater.* **2008**, *18*, 3850–3856.
38. Heller, H.; Ahrenstorf, K.; Broekaert Jose, A. C.; Weller, H. Investigation of the Nucleation and Growth Dynamics of FePt Nanoparticles Prepared *via* a High-Temperature Synthesis Route Employing PtCl(2) as Platinum Precursor. *Phys. Chem. Chem. Phys.* **2009**, *11*, 3257–3262.
39. Shevchenko, E. V.; Talapin, D. V.; Schnablegger, H.; Kornowski, A.; Festin, O.; Svedlindh, P.; Haase, M.; Weller, H. Study of Nucleation and Growth in the Organometallic Synthesis of Magnetic Alloy Nanocrystals: The Role of Nucleation Rate in Size Control of $CoPt_3$ Nanocrystals. *J. Am. Chem. Soc.* **2003**, *125*, 9090–9101.
40. Samia, A. C. S.; Hyzer, K.; Schlueter, J. A.; Qin, C.-J.; Jiang, J. S.; Bader, S. D.; Lin, X.-M. Ligand Effect on the Growth and the Digestion of Co Nanocrystals. *J. Am. Chem. Soc.* **2005**, *127*, 4126–4127.
41. Samia, A. C. S.; Schlueter, J. A.; Jiang, J. S.; Bader, S. D.; Qin, C.-J.; Lin, X.-M. Effect of Ligand−Metal Interactions on the Growth of Transition-Metal and Alloy Nanoparticles. *Chem. Mater.* **2006**, *18*, 5203–5212.
42. Murray, C. B.; Sun, S.; Doyle, H.; Betley, T. Monodisperse 3D Transition-Metal (Co, Ni, Fe) Nanoparticles and Their Assembly into Nanoparticle Superlattices. *MRS Bull.* **2001**, *26*, 985–991.
43. Dresselhaus, M. S.; Dresselhaus, G.; Jorio, A. Unusual Properties and Structure of Carbon Nanotubes. *Annu. Rev. Mater. Res.* **2004**, *34*, 247–278.
44. Chi, D. H.; Cuong, N. T.; Tuan, N. A.; Kim, Y.-T.; Bao, H. T.; Mitani, T.; Ozaki, T.; Nagao, H. Electronic Structures of Pt Clusters Adsorbed on (5,5) Single Wall Carbon Nanotube. *Chem. Phys. Lett.* **2006**, *432*, 213–217.
45. Cuong, N. T.; Chi, D. H.; Kim, Y.-T.; Mitani, T. Structural and Electronic Properties of Pt_n (n = 3, 7, 13) Clusters on Metallic Single Wall Carbon Nanotube. *Phys. Status Solidi B* **2006**, *243*, 3472–3475.
46. Durgun, E.; Dag, S.; Bagci, V., M. K.; Gulseren, O.; Yildirim, T.; Ciraci, S. Systematic Study of Adsorption of Single Atoms on a Carbon Nanotube. *Phys. Rev. B* **2003**, *67*, 201401/1–201401/4.
47. Bader, R. F. W. *Atoms in Molecules: A Quantum Theory*; Clarendon Press: Oxford U.K., 1990.
48. Becke, A. D.; Edgecombe, K. E. A Simple Measure of Electron Localization in Atomic and Molecular Systems. *J. Chem. Phys.* **1990**, *92*, 5397–5403.
49. Becke, A. D. Density-Functional Thermochemistry. III. The Role of Exact Exchange. *J. Chem. Phys.* **1993**, *98*, 5648–5652.
50. Lee, C.; Yang, W.; Parr, R. G. Development of the Colle-Salvetti Correlation-Energy Formula into a Functional of the Electron Density. *Phys. Rev. B* **1988**, *37*, 785–789.
51. http://bse.pnl.gov/bse/portal.
52. Hay, P. J.; Dunning, T. H., Jr. In *Methods of Electronic Structure Theory*; Schaefer, H. F., III, Ed.; Plenum: New York, 1977, Vol. 2.

53. Hay, P. J.; Wadt, W. R. *Ab Initio* Effective Core Potentials for Molecular Calculations. Potentials for the Transition Metal Atoms Scandium to Mercury. *J. Chem. Phys.* **1985**, *82*, 270–283.
54. Wadt, W. R.; Hay, P. J. *Ab Initio* Effective Core Potentials for Molecular Calculations. Potentials for Main Group Elements Sodium to Bismuth. *J. Chem. Phys.* **1985**, *82*, 284–298.
55. Hay, P. J.; Wadt, W. R. *Ab Initio* Effective Core Potentials for Molecular Calculations. Potentials for Potassium to Gold Including the Outermost Core Orbitals. *J. Chem. Phys.* **1985**, *82*, 299–310.
56. Hehre, W. J.; Stewart, R. F.; Pople, J. A. Self-Consistent Molecular-Orbital Methods. Use of Gaussian Expansions of Slater-Type Atomic Orbitals. *J. Chem. Phys.* **1969**, *51*, 2657–2664.
57. Although C atoms could be better described with a higher basis set, the minimal basis set STO-3G constitutes a suitable compromise between accuracy and computational performance, as we have previously reported that it reproduces accurately the geometries of CNTs, compared with other split-valence basis sets. See ref 58.
58. Martin-Martinez, F. J.; Melchor, S.; Dobado, J. A. Clar-Kekule Structuring in Armchair Carbon Nanotubes. *Org. Lett.* **2008**, *10*, 1991–1994.
59. In the configuration obtained in a previous single-point energy scan, with a Pt−Pt distance of 2.7 Å, which had been calculated before from an optimization of the isolated cluster. In the cluster−CNT optimization, we froze the coordinates of the platinum atoms, leaving the CNT free to relax. Thus, we avoided eventual deformations in the cluster and emulated a more real situation in which 14 Pt atoms are surrounded for others atoms in the NP, which restrict somehow their movement.
60. To make this scan systematic, we took the central atom of the 9 Pt array as a reference and placed it on the four different positions already explored for one Pt atom−CNT system. The three different orientations explored are at angles of 0, 30, and 45° between the cluster and CNT axis.
61. Du Pasquier, A.; Unalan, H. E.; Kanwal, A.; Miller, S.; Chhowalla, M. Conducting and Transparent Single-Wall Carbon Nanotube Electrodes for Polymer-Fullerene Solar Cells. *Appl. Phys. Lett.* **2005**, *87*, 203511/1–203511/3.
62. Durgun, E.; Dag, S.; Bagci, V. M. K.; Gulseren, O.; Yildirim, T.; Ciraci, S. Systematic Study of Adsorption of Single Atoms on a Carbon Nanotube. *Phys. Rev. B* **2003**, *67*, 201401/1–201401/4.
63. Frisch, M. J.; *et al. Gaussian 03*; Gaussian Inc.: Wallingford, CT, 2004.
64. Bylaska, E. J.; *et al. NWChem, A Computational Chemistry Package For Parallel Computers*, version 5.0; PNNL: Richland, WA 99352−09999, 2006.
65. Melchor, S.; Dobado, J. A. CoNTub: An Algorithm for Connecting Two Arbitrary Carbon Nanotubes. *J. Chem. Inf. Comput. Sci.* **2004**, *44*, 1639–1646.
66. http://www.ugr.es/local/gmdm/contub.htm.